

Contents lists available at ScienceDirect

Materialia

journal homepage: www.elsevier.com/locate/mtla



Anisotropic thermal conductivity of magnetocaloric AlFe₂B₂

Brian T. Lejeune a,b,*, Xinpeng Du d, Radhika Barua a, Ji-Cheng Zhao d, Laura H. Lewis a,b,c

- ^a Department of Chemical Engineering, Northeastern University, Boston, MA 02115, USA
- ^b George J. Kostas Research Institute for Homeland Security, Northeastern University, Burlington, MA 01803, USA
- ^c Department of Mechanical and Industrial Engineering, Northeastern University, Boston, MA 02115, USA
- ^d Department of Materials Science and Engineering, The Ohio State University, Columbus, OH 43210, USA



Keywords:
Thermal conductivity
Magnetic anisotropy
Ferromagnetic materials
Electron backscattering diffraction (EBSD)
Magnetocaloric



The thermal conductivity (κ) and heat capacity (C_p) of the magnetocaloric AlFe₂B₂ compound were investigated to assess its room temperature heat transfer and thermal management potential relative to other magnetocaloric materials such as FeRh, Gd, Gd₅(Si,Ge)₄ La(Fe,Si)₁₃ and (Mn,Fe) (P,As). The room temperature thermal conductivity was determined along the three principal crystallographic directions of AlFe₂B₂ using the time-domain thermoreflectance (TDTR) method on six randomly oriented AlFe₂B₂ grains, resulting in an observed anisotropic thermal conductivity with a 40% larger κ along the c-axis: κ_x = 4.7 \pm 0.1 W/mK, κ_y = 4.4 \pm 0.1 W/mK, and κ_z = 6.8 \pm 0.3 W/mK.

Primary energy that is not transformed into useful work typically takes the form of waste heat. In 2016, rejected thermal energy accounted for over 65% of all energy produced in the United States [1]. This scenario highlights the need for improved thermal energy management technologies, including new materials, to capture and transform waste heat into other usable forms of energy. The effectiveness of thermal energy harvesting devices is directly related to the heat transfer from the source to the harvester, for downstream use. Important parameters in this regard are the heat capacity (C_p) and the thermal conductivity (κ) of working materials in the energy harvesting device.

Included in the portfolio of materials for thermal energy management are magnetocaloric materials which undergo a reversible temperature change upon application and removal of an applied magnetic field [2] and are under consideration for application in solid-state refrigeration and thermal management devices. In this work we report the heat capacity and thermal conductivity of the intermetallic AlFe₂B₂ compound, to determine its near-room-temperature heat transfer potential. The AlFe2B2 (aka 1-2-2) system has recently become of interest to the scientific community due to the low cost of its constituent earth-abundant elements, relative ease of fabrication, promising tunable magnetocaloric effect near room temperature ($\Delta T_{ad} \sim 1.8$ –2.2 K at $\mu_0 H_{app} = 2$ T near $T \sim 290$ K) and low heat capacity ($C_p = 124$ J/mole K) [3–5]. The thermal transport behavior along with the previously reported anisotropic magnetic properties of AlFe₂B₂ [6] provide design considerations for incorporation of ${\rm AlFe_2B_2}$ -based compounds into heat transfer devices for thermal management.

The AlFe₂B₂ crystal structure (Fig. 1) consists of Al monolayers which alternate along the b-axis with Fe-B subunits that lie within the (ac)-plane. The intrinsic layered morphology of the AlFe₂B₂-type crystal structure donates a sizeable magnetocrystalline anisotropy of 0.9 MJ/m³ in the (ac)-plane [6-8]. Previous studies have reported that AlFe₂B₂ undergoes a coupled structural and magnetic phase transition in the vicinity of room temperature [9]. This magnetostructural phase transformation manifests as a non-uniform change in the lattice parameters with little change in the unit cell volume or crystal structure [9]. Although Cedervall et al. explicitly state that they detected no distortion in the 1-2-2 lattice at the magnetic phase transition temperature, their accompanying published data of the lattice parameters as a function of temperature appears to show a change in slope of the temperaturedependent lattice distortions in the vicinity of the phase transition temperature [10]. Recent publications have shown that the magnetocrystalline anisotropy leads to a larger magnitude of the magnetic entropy change when measured along the easy a-axis of AlFe2B2 versus the caxis and therefore the crystallographic orientation relative to the applied magnetic field is a useful magnetocaloric or thermal energy harvesting device design consideration [6]. Based on the anisotropic nature of the magnetocaloric effect in this system, it is of interest to determine the near-room-temperature anisotropic thermal conductivity (κ), and heat capacity (C_n) of AlFe₂B₂.

AlFe₂B₂ was synthesized by arc melting the constituent elements (99.9% purity) in a 1.5 Al: 2 Fe: 2 B molar ratio; excess Al was intentionally added to maximize the AlFe₂B₂ phase content and avoid

^{*} Corresponding author at: Department of Chemical Engineering, Northeastern University, Boston, MA 02115, USA. *E-mail address*: lejeune.b@husky.neu.edu (B.T. Lejeune).

B.T. Lejeune et al. Materialia 1 (2018) 150–154

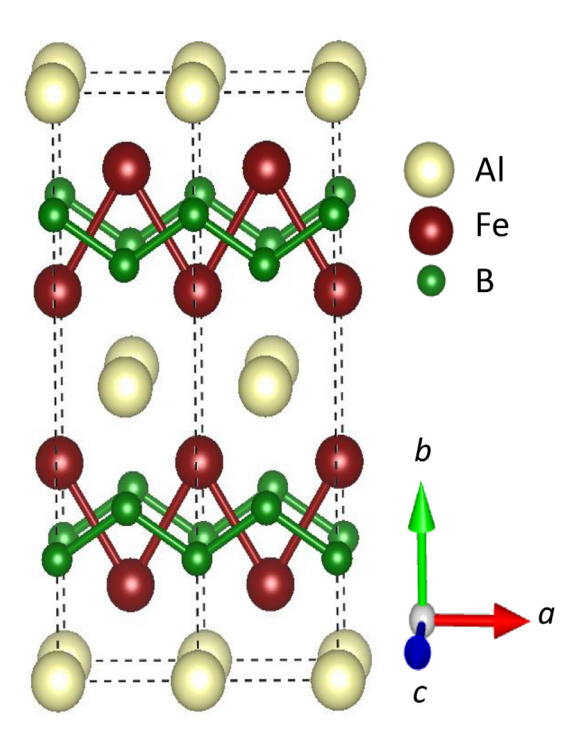


Fig. 1. AlFe₂B₂ crystal structure consisting of planes of Al atoms which act as spacers perpendicular to the long b-axis between Fe–B layers which lie in the (ac)-plane.

formation of deleterious iron borides [3]. Examination of the arc-melted charges using x-ray diffraction revealed AlFe₂B₂, Al₁₃Fe₄, and FeB. The arc-melted charges were subsequently pulverized in air with a mortar and pestle into a fine powder (<74 μ m), packed into a small diameter glass tube, which was closed on one end, and sealed under vacuum (1 \times 10⁻⁶ Torr) in a larger vitreous silica tube for annealing at 1000 °C for 7 days. Samples were furnace cooled following heat treatment. The annealed powders were etched while stirring continuously with 50%

v/v HCl for 13 min at room temperature to remove secondary Al-rich phases such as ${\rm Al}_{13}{\rm Fe}_{4,}$ delivering a higher phase fraction of ${\rm AlFe}_2{\rm B}_2.$ After etching, the powder was collected via vacuum filtration with a Buchner funnel. This purified ${\rm AlFe}_2{\rm B}_2$ powder was pressed at 1000 °C into a 2.54 cm-diameter disk and vacuum-sintered. This disk was sliced into slabs using a low-speed diamond saw for subsequent structural, magnetic and thermal transport characterization.

The chemical composition of the sintered disk was confirmed by probing three locations using scanning electron microscopy and energy-dispersive spectrometry (SEM-EDS, Hitachi S4800). The crystal structure of AlFe₂B₂ within the disk was again examined with x-ray diffraction (XRD, PANanalytical X' Pert PRO) using Cu-K $_{\alpha}$ radiation at room temperature in the angular range $10^{\circ} \leq 2\theta \leq 80^{\circ}$ Bragg reflections obtained from the x-ray diffraction patterns were fit with a pseudo-Voight function and successfully indexed to an orthorhombic unit cell using a least-squares cell-parameter refinement method [11].

A small piece of the AlFe₂B₂ sintered disk was removed using electrical discharge machining (EDM) and mounted in copper-based bakelite for thermal conductivity measurements. The surface of the mounted sample was subsequently ground in water using SiC paper of 120, 320, 600, 800, 1200 grit sizes in sequence and was then polished for 24 h with a vibratory polisher using 0.05-µm colloidal silica suspension. Several indents were put into the surface of the polished sample with a micro-indenter (Buehler Micromet II Digital Micro Hardness Tester) to mark selected regions (~ 400 × 600 μm) for electron backscatter diffraction (EBSD, XL-30 ESEM system (FEI, Inc.)) characterization and subsequent thermal conductivity measurements. The lattice parameters of AlFe₂B₂ and the Wyckoff positions of the constituent atoms published by Jeitschko were applied into the TSL OIM analysis software to simulate electron diffraction patterns (Kikuchi patterns), which were used to determine orientations of local grains through fitting the experimental Kikuchi patterns from EBSD [8]. In this manner, the crystallographic orientation of each grain was obtained, as shown in the inverse pole orientation map (Fig. 2) of the AlFe₂B₂ microstructure in the selected region (area 400×600 μm), utilizing the Euler angle data provided by EBSD. This information was used to determine the thermal transport directions of thermal conductivity measurements, represented as the direction cosines relative to the crystalline principle axes. Six of the

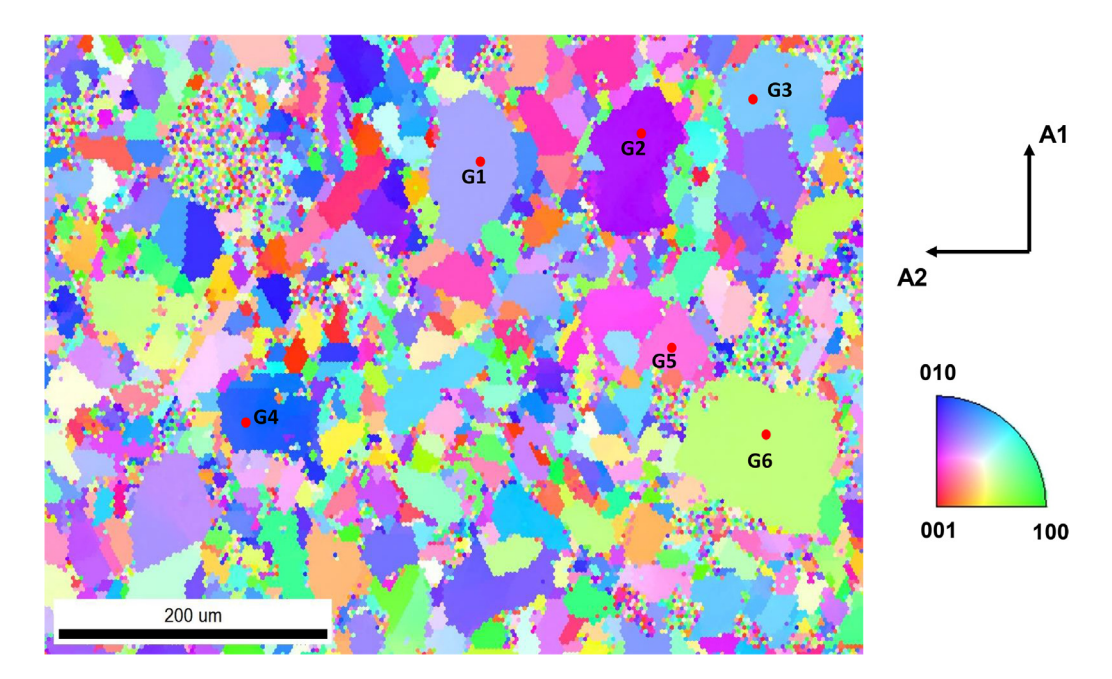


Fig. 2. Inverse pole figure [001] obtained from the EBSD experiment on the selected $400 \times 600 \, \mu m$ region. The multicolored regions represent orientations identified based on the scale shown on the right. Sample coordinate frame (A1 and A2 axes) is also given. Six larger grains labelled from G1 to G6 with distinct anisotropic orientations were selected for subsequent TDTR experiments.

B.T. Lejeune et al. Materialia 1 (2018) 150–154

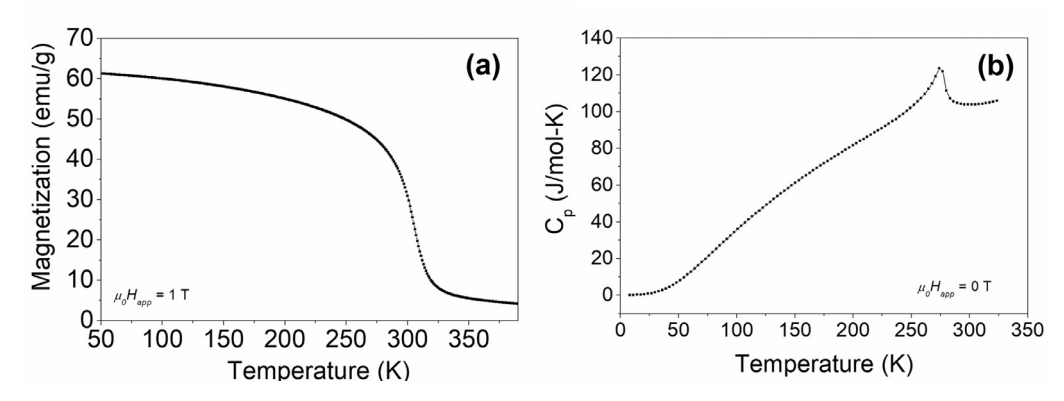


Fig. 3. (a) Temperature-dependent magnetization (M(T)) of the AlFe₂B₂ sintered disk at $\mu_0 H_{app} = 1$ T showing a Curie temperature of 305 K (b) Zero-field heat capacity (C_n) as a function of temperature in the temperature range of 8 K < T < 325 K.

large grains, labeled as G1–G6 in Fig. 2, (roughly $50-70\,\mu m$ in diameter) were chosen for subsequent thermal conductivity measurements using the TDTR method.

Magnetic characterization of the AlFe₂B₂ sintered disk (Fig. 3(a)) led to determination of the Curie temperature ($T_C = 305 \, \mathrm{K}$ @ 1 T) and saturation magnetization ($M_S = 70.8 \, \mathrm{emu/g}$). By comparing the experimental saturation magnetization M_S value with values reported in the literature for AlFe₂B₂ and FeB it was determined that the phase fractions of AlFe₂B₂, FeB, and Al-rich phases (non-magnetic) were 87%, 5%, and 8% by weight respectively [4,5]. Heat capacity measurements (Fig. 3(b)) were performed in zero applied magnetic field using a Physical Property Measurement System (PPMS, Quantum Design) in the temperature range of 8 K < T < 325 K.

The thermal conductivity of the sample was measured at $291 \pm 2 \,\mathrm{K}$ using TDTR within the six large grains whose orientations were previously determined by EBSD. A film of aluminum of ~95 nm in thickness was first sputter-deposited at room temperature onto the surface of the polished sintered sample for 420 s (conditions: 30 W DC power; 3×10^{-7} Torr vacuum) to act as the transducer for TDTR measurements. A femtosecond laser was split into the pump and probe beams. The pump beam was used to deposit heat on the sample surface and the probe beam was used to detect the change of the thermal reflectance as heat was being conducted away from the surface by the sample. Both beams arrived on the same position on the sample surface but at different times. The thermal reflectance change as a function of the time delay between the pump and probe beams was fitted through a thermal transport model, from which the thermal conductivity (κ) on the local grain orientation was extracted using the density taken as 5.75 g/cm³ [8] and the heat capacity (C_n) value determined earlier. Details regarding the data fitting procedure for obtaining the thermal conductivity using the TDTR technique can be found in prior publications [12,13]. For each anisotropic direction within the grain, as determined by EBSD, 5-8 measurements were conducted. The thermal conductivity along any given direction relative to the principle axes of the orthorhombic 1-2-2 structure can be expressed as follows:

$$\kappa = l_1^2 \kappa_x + l_2^2 \kappa_y + l_3^2 \kappa_z \tag{1}$$

where l_i is the direction cosine along the ith direction and κ_x , κ_y , κ_z are the thermal conductivities along the principle axes of the lattice [14]. Based on the determined thermal conductivity κ of the six randomly oriented chosen grains in the polished 1-2-2 sample and their direction cosines, the unknown's κ_x , κ_y , κ_z were extracted using a pseudo-inverse algorithm as described in references [15–17].

The x-ray diffraction pattern (Fig. 4) of the sintered sample overlaid with the reference diffraction Bragg peak data for AlFe₂B₂ (shown in green) and FeB (shown in blue) contains diffraction peaks corresponding primarily to AlFe₂B₂ (a = 2.927(1) Å, b = 11.043(4) Å, c = 2.870(1) Å), with several low-intensity peaks associated with minor amounts of the

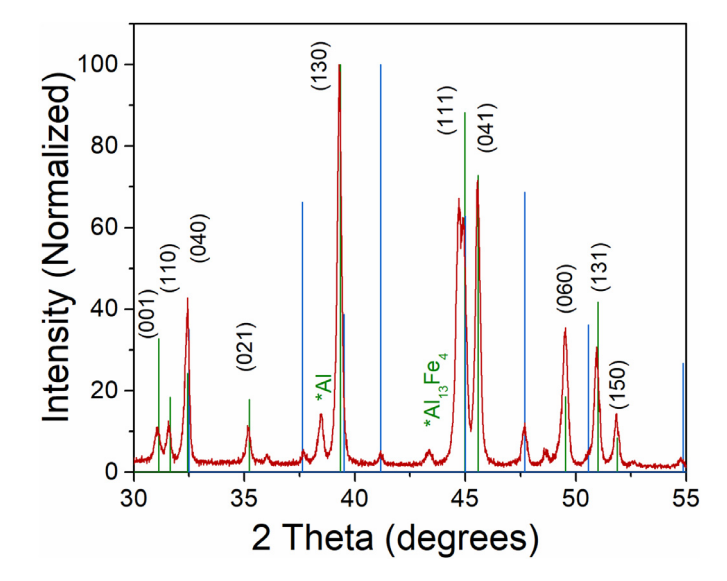


Fig. 4. X-ray diffraction pattern of the $AlFe_2B_2$ sintered sample overlaid with standard diffraction data for $AlFe_2B_2$ (green) and FeB (blue) showing diffraction peaks corresponding primarily to $AlFe_2B_2$ with minority phase peaks associated with FeB, Al, and $Al_{13}Fe_4$. (For interpretation of the references to color in this figure legend, the reader is referred to the web version of this article).

Al, $Al_{13}Fe_4$, and FeB phases. The significant breadth of x-ray diffraction peaks is attributed to disordering and surface roughness from the sintering process since the sample was not polished prior to x-ray diffraction measurements. The Al: Fe atomic ratio within this sample was confirmed as $\sim 1:2$ consistent with that expected for the 1-2-2 phase.

The heat capacity (C_p) of AlFe₂B₂ was found to increase with increasing temperature from 8 K to 325 K with a peak observed in the vicinity of the magnetic phase transition ($T_C \sim 290$ K) that reached a maximum C_p of 123 J/mol-K. This C_p peak has a magnitude $\sim 15\%$ larger than the baseline C_p value in its vicinity with a width of ~ 15 –20 K. The thermal conductivities (κ) for the six largest grains (G1–G6) of AlFe₂B₂ in the characterized region (Fig. 2), along with their direction cosines, are provided in Table 1.

The thermal conductivity (κ) of grains G1 through G6, along with the crystallographic orientations of these grains, allows determination of the anisotropic thermal conductivity values of AlFe₂B₂: $\kappa_{\rm x} = 4.7 \pm 0.1$ W/mK, $\kappa_{\rm y} = 4.4 \pm 0.1$ W/mK, and $\kappa_{\rm z} = 6.8 \pm 0.3$ W/mK. The magnitude of κ along the c-axis is over 40% larger than the values measured along the a- and b-axes. The c-axis is normal to B–B chains within the Fe–B layer of the crystal structure which could act as an insulating barrier, thus inhibiting heat transfer, contributing to the

B.T. Lejeune et al. Materialia 1 (2018) 150–154

Table 1The measured thermal conductivity of the six grains G1 to G6 along with their positions, Euler angles, and direction cosines used to determine the thermal conductivity along all three crystallographic directions.

Grain	Position (µm)	Euler Angle (Bunge's convention)	Direction cosines relative to the principal crystallographic axes	Thermal conductivity (W/m-K)
G1	(320, 80)	(202.7, 68.8, 333.0)	[-0.4233 0.8307 0.3616]	4.4 ± 0.1
G2	(440, 60)	(181.0, 60.8, 359.6)	[-0.0061 0.8729 0.4879]	3.8 ± 0.2
G3	(520, 40)	(152.5, 101.8, 214.4)	[-0.5530 -0.8077 -0.2045]	6.3 ± 0.2
G4	(150, 250)	(1.1, 89.0, 191.5)	[-0.1993 -0.9798 0.0175]	4.1 ± 0.2
G5	(460, 200)	(169.4, 135.4, 198.0)	[-0.2170 - 0.6678 - 0.7120]	6.4 ± 0.2
G6	(530, 260)	(177.8, 61.1, 72.5)	[0.8349 0.2633 0.4833]	4.5 ± 0.1

Table 2 Transition temperature (T_t) , heat capacity (C_p) , and thermal conductivity (κ) for AlFe₂B₂ and other candidates for near-room-temperature magnetic cooling.

Material	T_t (K)	Cp (J/mol-K)	κ (W/m-K)	Reference
AlFe ₂ B ₂	280-310	123	6.8	[9]
FeRh	360-400	90	6.1 (AFM); 9.3 (FM)	[19-21]
Gd	295	52-100	10	[2,22,23]
Gd ₅ (Si,Ge) ₄	276-335	90	6	[2,23,24]
La(Fe,Si) ₁₃	287-356	900	10-15	[2,22,23,25,26]
Mn-Fe-As-P	260–318	300	2	[2,23,27]

anisotropic thermal behavior observed. Further, the enhanced thermal conductivity direction is perpendicular to the easy axis of magnetization (*a*-axis) [6]. The isotropic thermal conductivity based on κ_x κ_y and κ_z (Eq. [1]) is determined as $5.2 \, \text{W/mK} \pm 0.3$.

These attributes impact contemplation of $AlFe_2B_2$ -based materials as working materials in near-room-temperature thermal energy management devices, including magnetic refrigeration devices. An efficient thermal regenerator should transfer heat from the interior of a region to the heat transfer fluid at a sufficiently high rate as well as minimize heat transfer radiating away from the intended path of heat transfer. Thus an ideal regenerator material should possess a significantly larger thermal conductivity in the direction of the heat transfer fluid's path and low thermal conductivity in the transverse direction [18]. Our results indicate that, if properly textured and/or aligned, $AlFe_2B_2$ may be used to optimize the heat transfer efficiency of a potential cooling device.

The heat capacity (C_p) determined for $AlFe_2B_2$ is found to be comparable with those of other materials under consideration as room temperature magnetocaloric materials, such as FeRh, Gd, and $Gd_5(Si,Ge)_4$, with values listed in Table 2. The measured $AlFe_2B_2$ C_p is substantially lower than that reported for the $La(Fe,Si)_{13}$ and (Mn,Fe)P systems, an aspect that is beneficial from a heat removal standpoint. An additional consideration for near-room-temperature thermal property assessment is the magnitude of the C_p peak in the vicinity of T_c when the magnetic transition is near room temperature. The magnitude of the C_p peak for $AlFe_2B_2$ (123 J/mol-K) is on the order of 15% of the baseline value (103 J/mol-K) at temperatures above and below the peak, which is similar to Gd and significantly smaller than observed in FeRh, $Gd_5(Si,Ge)_4$, $La(Fe,Si)_{13}$ and (Mn,Fe)P systems where the C_p peak is twice as large as the baseline [19,22,23].

The measured AlFe₂B₂ thermal conductivity (κ) near room temperature is comparable to the values that characterize FeRh, Gd, Gd₅(Si,Ge)₄, and La(Fe,Si)₁₃ and is once again significantly larger that reported for the (Mn,Fe)P system. Note that the peak in C_p may manifest itself in the thermal conductivity and/or thermal diffusivity as noted by Fujieda et al. when calculated near T_c [23]. In the case of the measurement results presented in this work the small magnitude of the peak in C_p reported above reduces the potential deviations in κ near room temperature for AlFe₂B₂ due to the T_c . The C_p peak value (123 J/mol-K) was used for κ calculations, which provides a conservative estimate of κ in the vicinity of T_C . Typically in the AlFe₂B₂ system the specific heat (C_p) peak appears \sim 10–15 K below T_C (305 K) and the width of this peak is only \sim 15–20 K, therefore for near-room-temperature applications κ

may be up to 15% larger when above and below T_c making AlFe₂B₂ even more competitive with other thermal management materials.

In summary, investigation and comparison of the heat capacity and thermal conductivity of AlFe₂B₂ with other magnetocaloric materials such as FeRh, Gd, Gd₅(Si,Ge)₄ La(Fe,Si)₁₃ and (Mn,Fe)(P,As) has identified it as a promising candidate material from a heat transfer perspective for refrigeration and thermal management devices. The room temperature anisotropic thermal conductivity observed: $\kappa_{\rm x}=4.7\pm0.1\,\rm W/mK$, $\kappa_{\rm y}=4.4\pm0.1\,\rm W/mK$, and $\kappa_{\rm z}=6.8\pm0.3\,\rm W/mK$, which is 40% larger along the c-axis, may be leveraged to enhance heat transfer when this material is crystallographically-oriented prior to incorporation into a device. The low cost and abundance of the elemental constituents in AlFe₂B₂ in combination with its comparable thermal properties relative to other magnetocaloric materials make this material of interest for thermal management applications such as magnetic refrigeration and energy harvesting.

Acknowledgment

This work was supported by Northeastern University; the U.S Department of Energy [grant number DE-AR00000754]; The TDTR measurement at Ohio State was funded U.S. National Science Foundation [grant number NSF-DMR-1237577].

Declarations of interest

none

References

- Annual United States energy flow chart: https://flowcharts.linl.gov/ (Accessed in April 2018).
- [2] V. Franco, J.S. Blázquez, B. Ingale, A. Conde, Annu. Rev. Mater. Res. 42 (2012) 305.
 [3] X. Tan, P. Chai, C.M. Thompson, M. Shatruk, J. Am. Chem. Soc. 135 (2013) 9553.
- [3] X. Tan, P. Chai, C.M. Thompson, M. Shatruk, J. Am. Chem. Soc. 135 (2013) 9553.
 [4] M. ElMassalami, D.D.S. Oliveira, H. Takeya, J. Magn. Magn. Mater. 323 (2011) 2133.
- [5] E.M. Levin, B.A. Jensen, R. Barua, B. Leieune, A. Howard, R.W. McCallum,
- M.J. Kramer, L.H. Lewis, Phys. Rev. Mater. 2 (2018) 1.
- [6] R. Barua, B.T. Lejeune, L. Ke, G. Hadjipanayis, E.M. Levin, R.W. McCallum, M.J. Kramer, L.H. Lewis, J. Alloys Compd. 745 (2018) 505.
- [7] L. Ke, B.N. Harmon, M.J. Kramer, Phys. Rev. B 95 (2017) 1.
- [8] W. Jeitschko, Acta Crystallogr. B25 (1969) 163.
- [9] L.H. Lewis, R. Barua, B. Lejeune, J. Alloys Compd. 650 (2015) 482.
- [10] J. Cedervall, M. Svante, T. Sarkar, E.K. Delczeg-czirjak, L. Bergqvist, T.C. Hansen, P. Beran, P. Nordblad, M. Sahlberg, J. Alloys Compd. 664 (2016) 784.
- [11] G.A. Novak, A.A. Colville, Am. Mineral. 74 (1989) 488.

B.T. Lejeune et al. Materialia 1 (2018) 150-154

- [12] S. Huxtable, D.G. Cahill, V. Fauconnier, J.O. White, J.C. Zhao, Nat. Mater. 3 (2004)
- [13] X. Zheng, D.G. Cahill, P. Krasnochtchekov, R.S. Averback, J.C. Zhao, Acta Mater. 55 (2007) 5177.
- [14] J.F. Nye, Physical Properties of Crystals: Their Representation by Tensors and Matrices, 2nd ed., Oxford university press, New York, 1985.

 [15] A. Bjerhammar, Trans. R. Inst. Technol. Stock. 49 (1951) 1.

- [16] E.H. Moore, Bull. Am. Math. Soc. 26 (1920) 394.
 [17] R. Penrose, J.A. Todd, Math. Proc. Camb. Philos. Soc 51 (1955) 406.
 [18] A. Kitanovski, J. Tušek, U. Tomc, U. Plaznik, M. Ožbolt, A. Poredoš, in: Magnetocaloric Energy Convers., Springer International Publishing, 2015, 23.
- [19] D.W. Cooke, F. Hellman, C. Baldasseroni, C. Bordel, S. Moyerman, E.E. Fullerton, Phys. Rev. Lett. 109 (2012) 7.
- [20] C.J. Schinkel, R. Hartog, F.H.A.M. Hochstenbach, J. Phys, F Met. Phys. 4 (1974) 1412

- [21] S. Maat, J.U. Thiele, E.E. Fullerton, Phys. Rev. B Condens. Matter Mater. Phys. 72 (2005) 1.
- [22] R. Bjørk, C.R.H. Bahl, M. Katter, J. Magn, Magn. Mater. 322 (2010) 3882.
 [23] S. Fujieda, Y. Hasegawa, A. Fujita, K. Fukamichi, J. Appl. Phys. 95 (2004) 2429.
- [24] V.K. Pecharsky, K.A. Gschneidner, Phys. Rev. Lett. 78 (1997) 4494.
- [25] A. Barcza, M. Katter, V. Zellmann, S. Russek, S. Jacobs, C. Zimm, IEEE Trans. Magn. 47 (2011) 3391.
- [26] J. Liu, J.D. Moore, K.P. Skokov, M. Krautz, K. Löwe, A. Barcza, M. Katter, O. Gutfleisch, Scr. Mater. 67 (2012) 584.
- [27] E. Brück, O. Tegus, D.T. Cam Thanh, N.T. Trung, K.H.J. Buschow, Int. J. Refrig. 31 (2008) 763.